

**A Monte Carlo Study of the Structural Properties of
End-linked Polymer Networks**

Nisha Gilra, Claude Cohen

*School of Chemical Engineering,
Cornell University,
Ithaca, NY 14853, USA*

and A.Z. Panagiotopoulos*

*Institute for Physical Science and Technology and
Department of Chemical Engineering,
University of Maryland, College Park 20742, USA*

* To whom correspondence should be addressed. Electronic mail: thanos@ipst.umd.edu

Abstract

The formation and structural properties of end-linked polymer networks were studied in the framework of the bond fluctuation model on a three-dimensional cubic lattice. Only excluded volume interactions were considered between repeat units (monomers and cross-links). Networks were created with a wide range of the ratio of cross-link sites to precursor polymer chain ends, r , to test the experimental observation that a non-stoichiometric ratio generates a more perfect network. Systems of 10-, 20-, and 50-mer precursor polymer chains with values of r ranging from 0.9 to 1.6 were studied. An algorithm was developed to determine the soluble fraction and the amount of loops and pendent structures. The network properties were evaluated at the same number of Monte Carlo steps per repeat unit for each chain length independent of r value. In agreement with experimental observations, the simulation results show that the optimum r values are non-stoichiometric, increase with increasing chain length of the precursor polymer chain, and increase with side reaction.

Introduction

The molecular architecture of polymer networks strongly influences their mechanical and chemical behavior. An ideal, model end-linked network is one in which all of the precursor polymers become elastic chains¹. In real networks, however, imperfections cause the elastic properties of the networks to diminish. These imperfections include pendent structures, which are attached to the network at only one end, and loops. It is desirable to determine the conditions at which these microscopic network defects are minimized so that macroscopic properties such as the elastic modulus can be optimized. One parameter that can be optimized is the ratio of number of cross-link sites available for reaction divided by the number of chain ends available for reaction, r .

It was experimentally determined with model end-linked poly(dimethylsiloxane) networks¹ and with end-linked poly(tetrahydrofuran) networks², that a non-stoichiometric ratio generates a network with a lower soluble fraction and a higher elastic modulus indicating a more defect-free network. This effect may occur because cross-links react with themselves in a side reaction³⁻⁵ or because kinetic limitations prevent systems at low r values to achieve high extents of reaction¹. It was also determined that the r value at which the networks' defects are minimized, r_{opt} , was dependent on the precursor polymer molecular weight², such that as the precursor molecular weight was increased, the r_{opt} would shift to a higher r value.

Computer simulation has become a powerful tool to study network physical properties because it can be used to characterize the network on a microscopic level, providing information that is difficult or impossible to collect experimentally. Various

computer simulation studies of polymer networks have been performed⁶⁻²⁴. One of the earliest studies⁶⁻⁷ of network formation was performed using a static cross-linking method to obtain structural properties of tetrafunctional and trifunctional end-linked networks. These researchers measured the soluble fraction and network imperfections, including dangling chains, loops, and dangling loops. They also varied the ratio of cross-links to precursor chain ends between $r = 0.8$ and $r = 1.2$ and found that the most perfect networks were obtained when $r = 1.0$, when the networks were compared at the same extents of reaction. Other simulation studies⁸⁻⁹ of the structural properties of stoichiometric, end-linked networks were performed using Monte Carlo simulations. The influence of different reaction times on the kinetics of formation and the structure and swelling of the resulting networks was determined. The soluble fraction, and network imperfections including the dangling chains, loops, and dangling loops were found to depend only on the precursor polymer chain length, not on the reaction speed.

In this work, we have studied the formation of end-linked polymer networks with a range of precursor polymer chain lengths and cross-link concentrations using Monte Carlo simulations. Specifically, we have studied precursor polymer chain lengths of 10-, 20-, and 50-mer with values of r ranging from 0.9 to 1.6. To the best of our knowledge, the effect of the ratio, r , on network properties has not been previously studied by a dynamic simulation.

We have investigated the resulting network molecular architecture with a method we developed that catalogs the connectivity of the network and allows for the calculation of the soluble fraction and network imperfections, including pendent material and loops. Using this method, we have determined the optimum r value that minimizes network

defects for the networks studied. We have also studied the effect of incorporating a side reaction between cross-links during the cure on r_{opt} of the resulting network.

Model and Simulation Methodology

Model

The polymer networks were studied using the bond fluctuation model²⁵⁻²⁷ in three dimensions on a simple cubic lattice. This coarse-grained lattice algorithm is widely used for the simulation of dense polymer systems²⁸, including polymer networks^{8-10,14-17,24}. Monomers and cross-links, both considered to be repeat units, are modeled as occupying eight lattice sites. The repeat units are connected by bond vectors whose lengths vary in such a way that both the local self-avoidance of the chains is guaranteed and the chains are prevented from crossing each other in the course of their motion. There are six classes of bond vectors available: [2,0,0], [2,1,0], [2,1,1], [2,2,1], [3,0,0], and [3,1,0]. Permutation and sign combination of these classes of bond vectors leads to a combination of 108 different bond vectors with five different choices for the bond length.

The random motion of the chains is modeled by a diffusive hop where a repeat unit is chosen at random and displaced a lattice constant in an arbitrary lattice direction. The move is accepted if the neighboring lattice sites in the direction of the move are empty and if the resulting new bond vectors are in the set of five available bond lengths. This model is appropriate for studying dense systems because each eight-site repeat unit requires only four vacant lattice sites to successfully execute a move²⁶, which allows for both the difunctional monomers and the multifunctional cross-links to exhibit mobility⁹.

Since we are interested only in the structural properties of the networks, we have studied the networks in an athermal setting where only excluded volume interactions and connectivity are considered between repeat units. We studied the systems with a volume fraction ranging from around 0.46 to 0.48, which has been previously established to correspond approximately to polymer melt densities^{8,27}.

Simulation Methodology

The systems were created by adding tetrafunctional cross-links to monodisperse polymer melts. For the 10- and 20-mer systems, we used a 60x60x60 lattice and for the 50-mer system, we used a 95x95x95 lattice. Periodic boundary conditions were imposed in the x and y dimensions and hard walls were placed in the z dimension to allow for deformation simulations at some later time. The volume fraction is defined as:

$$\mathbf{f} = \frac{8\mathbf{u}(LM + C)}{V} \quad (1)$$

where L = the number of monomers per precursor chain, M = the number of precursor chains, C = the number of cross-links, \mathbf{u} = the volume of a lattice site, V = the lattice volume, and 8 is the constant representing that each repeat unit occupies eight lattice sites. For this tetrafunctional end-linked system, $r = 2C/M$.

The 10-mer networks were generated with 1225 precursor chains and r values of 0.9, 1.0, 1.05, 1.2, and 1.4. The 20-mer networks were created with 612 precursor chains and r values of 0.9, 1.0, 1.05, 1.2, and 1.4. The 50-mer networks were created with 968 precursor chains with r values of 0.9, 1.0, 1.2, 1.4, and 1.6 for the systems without side reaction, and with r values of 1.0, 1.1, 1.2, 1.4, 1.6, 1.8, 2.0, 2.4, and 3.0 for systems with

side reaction. Each simulation for all of the chain lengths at the various r values was performed four times in order to get error estimates.

The initial configurations were created using the unrestricted set of six bond vectors in the bond fluctuation model. These initial configurations have a small fraction (less than 1%) of immobile monomers because the three bond vectors ($[2,2,1]$, $[3,0,0]$, $[3,1,0]$), which allow for the bond lengths of 3 and $\sqrt{10}$, can cause two polymer chains to intertwine and create an immobile knot²⁷. We re-ran several of the simulations in an identical fashion except that the initial configuration was created with a restricted set of bond vectors ($[2,0,0]$, $[2,1,0]$, and $[2,1,1]$), which eliminates immobile knots. We found that the absence of these knots in the initial configuration does not change the qualitative results of the structural properties of interest of the networks and that the quantitative results are the same within statistical uncertainties.

The system was equilibrated using monomer and cross-link displacement moves. Such a move is one where either a monomer or a cross-link is attempted to relocate to one of six nearest neighbor positions. The move was accepted if the lattice position was unoccupied and the new bond vector was in the class of available bond vectors in the bond fluctuation model. The equilibration period was approximately 7,800 Monte Carlo steps per repeat unit (MCS/RU) for the 10-mer system, 23,900 MCS/RU for the 20-mer system, and 163,700 MCS/RU for the 50-mer system. During the equilibration phase, no reaction was allowed to occur.

When the cure was started, a bond was allowed to form when an unsaturated chain end or cross-link moved into one of each other's six nearest neighbor positions.

It was determined in previous work⁸ that the reaction probability with which a bond was formed did not affect the evolution of the soluble fraction or the network imperfections during the cure. Therefore, since the reaction probability in these systems determined the speed at which the network cured and did not affect the properties of interest, a reaction probability of unity was chosen. The network was allowed to cure until a specified number of Monte Carlo steps per repeat unit, denoted by t_{cure} , was reached. Stopping the cure at t_{cure} more closely resembles experimental protocol than stopping the cure at a specified extent of reaction, because experimentally, the reaction is stopped after a specific time has elapsed. The chosen t_{cure} was set as a constant value for all r values studied for a given chain length.

The simulation of the cure with a side reaction was performed slightly differently. Instead of allowing unsaturated cross-links to only bond with unreacted chain-ends, they were also allowed to bond with other unsaturated cross-links with a specified probability. This probability, P_x , was set to be 0.25 for these simulations. We studied the effect of the side reaction with the 50-mer networks as the representative system.

Determining network properties

We evaluated the structural properties of the resulting networks by first determining their soluble fractions. We created a method to determine the soluble fraction by tracing a route of connected chains and cross-links within the network. This method is loosely based on the SPANFO²⁹ algorithm in that it uses the same type of input parameters. The soluble fraction is defined as:

$$w_{sol} = 1 - \frac{nL + m}{LM + C} \quad (3)$$

where n = the number of network chains and m = the number of network cross-links.

Furthermore, we developed a method to determine the pendent material in the network. It is implemented as follows:

- 1) Start at any of the terminal points of the network. If there is only ONE path from a terminal point to the network, the whole structure is pendent. A pictorial representation of the terminal points are shown in Figure 1 and they are defined as follows:
 - a) an end-capped chain - a chain that has a single-functional cross-link attached to one of its chain ends and is attached to the network at the other end.
 - b) a dangling loop - a chain which is connected twice to the same cross-link that is attached to the network.
 - c) a dangling chain - a single chain that is connected to only one cross-link that is attached to the network.
- 2) Trace the route until a cross-link is found that has more than one connection to other chains that are not pendent material. Keep track as to which chains and cross-links have been visited to avoid over counting of pendent material.
- 3) Count any single-chain loops that are found along the way as part of the pendent material.
- 4) Include specific sites of the cross-links that are attached to pendent chains in the calculation of the pendent material³⁰.

Long connected pendent chains and branched pendent structures can be calculated using this method. Any loops that have more than one chain are not included.

Single-chain loops attached to the elastic network rather than to large pendent structures are also not considered elastic material¹¹⁻¹³. The number of these loops was calculated by determining the number of chains that were connected at both ends to the same cross-link and that were not part of larger pendent material. Then, the fraction of the elastically effective material is:

$$w_{elast} = 1 - w_{sol} - w_{pend} - w_{loops} \quad (4)$$

where w_{pend} is the fraction of pendent material and w_{loops} is the fraction of single-chain loops attached to the elastic network.

Results & Discussion

Evolution of the Network Properties

We present the network properties of the 50-mer networks as a representative system as they evolve during the cure as a function of Monte Carlo step per repeat unit. The data in all of the following figures is the average of four independent runs and representative error bars are shown. In Figure 2, the fraction of unreacted chain ends is plotted versus MC step per repeat unit for all the values of r examined. The fraction of unreacted chain ends during the cure of the network for $r = 1$ is expected to decay as a power law in time t^{-a} with $a \sim 0.5$ at intermediate times¹². Although time is not a quantity that is inherently present in Monte Carlo simulations, Monte Carlo steps can be considered to be proportional to time. Trautenberg, et al.⁸ verified this behavior with their Monte Carlo study of the 10- and 20-mer networks on a 123x123x123 lattice. We used smaller system sizes depending on precursor chain length to decrease the CPU time to cure the networks. In order to justify using the smaller system size, we monitored the

fraction of unreacted chain ends as the reaction proceeded. We found that for the 10- and 20-mer systems on the 60x60x60 lattice, the fraction of unreacted chain ends matched the literature data for the 123x123x123 lattice. Also, the 50-mer networks on the 95x95x95 system followed the expected behavior and exhibited a ‘time’ regime where the fraction of unreacted chain ends decayed $\sim t^{-0.5}$. The small, straight line shown on Figure 2 represents a slope equal to -0.5.

Figure 2 indicates that the cure proceeds more rapidly as r is increased. For $r = 0.9$ and 1.0 , the decay to the final state is significantly slower than for $r > 1.0$, an effect that is to be expected¹². In fact, the extent of reaction approaches unity for $r = 1.6$ by the end of the run.

In Figures 3 to 6, the behavior of individual network properties is shown as a function of the number of MC steps per repeat unit for the 50-mer networks for a range of r values. Figure 3 shows the evolution of the soluble fraction and shows that the minimum soluble fraction is reached with $r = 1.2$. The soluble fraction for $r = 0.9$ and 1.0 is slowly decreasing while for $r > 1.0$ has reached a relatively constant value. In Figure 4, the behavior of the fraction of pendent material is shown. This property goes through a maximum and then levels off for $r > 1$ and slowly decreases for $r \leq 1$. The minimum value of the fraction of pendent chains is exhibited with $r = 1.2$. As can be seen in Figure 5, the fraction of single-chain network loops increases as the cure progresses and appears to level off for $r = 1.4$ and 1.6 , but continues to increase slowly for $r \leq 1.2$. The highest value for w_{loops} is obtained for $r = 1.0$ with intermediate values observed when $r = 0.9$ and 1.2 and the lowest value for $r = 1.6$. The fraction of elastic chains continually increases as is shown in Figure 6. The largest fraction of elastic chains

is present for $r = 1.2$. Although, the w_{elast} for $r = 1$ is steadily increasing and looks as if it may overtake the fraction of elastic chains for $r = 1.2$, it has not done so in a reasonable cure time.

Just like in an experiment, it is unrealistic to allow the cure to continue for an infinite time, so an appropriate stopping time was determined. This t_{cure} was determined separately for each chain length, as the time beyond which the soluble fraction and network defects "ceased changing significantly". The slow evolution of the system beyond a certain time can be seen in Figures 3 - 6. Somewhat arbitrarily, t_{cure} was chosen to be 370,000 MCS/RU for the 50-mer system, 159,000 MCS/RU for the 20-mer system and 155,000 MCS/RU for the 10-mer system. The cure of the 50-mer systems that incorporated a side reaction was stopped at a t_{cure} value of 205,000 MCS/RU, which is less than for the 50-mer system without side reaction because the cross-link sites available for reaction were depleted more rapidly. These chosen values of t_{cure} do not strongly affect the qualitative conclusions of the behavior of the structural and elastic properties of the resulting networks.

Structural Properties of the Network

In Figures 7 to 11, the network properties are plotted for all three chain lengths at their respective t_{cure} values. The lines drawn through the data in these figures are guides for the eye and representative error bars are shown. In Figure 7, the weight fraction of soluble material is plotted vs. r . The soluble fraction goes through a minimum value for all chain lengths studied. There is an increased w_{sol} for $r < r_{opt}$ caused by unreacted chain ends due to lack of cross-links. Also, there is an increased w_{sol} for $r > r_{opt}$ because the

overabundance of cross-links causes end-capping of pendent network chains and of soluble chains rendering them unreactive. For the 10-mer networks, r_{opt} is between $r = 1 - 1.05$, for the 20-mer networks between $r = 1.05 - 1.2$, and for the 50-mer networks at $r = 1.2$. Minimum soluble fractions for all chain lengths are less than 1%, indicating that the networks are close to being model networks⁵. Furthermore, the values for r_{opt} indicate that minimum values are found at non-stoichiometric ratios. Also, as the precursor chain length is increased, the r_{opt} shifts to higher r values. Both these findings corroborate experimental evidence¹⁻².

Figure 8 shows the fractions of pendent material as a function of r . Here it can be seen that the r value at which w_{pend} is a minimum is $r = 1.05$ for the 10-mer networks, between $r = 1.05 - 1.2$ for the 20-mer networks, and at $r = 1.2$ for the 50-mer networks. The lack of cross-links generate dangling chains for $r < 1$ and the abundance of cross-links create pendent end-capped structures for $r \gg 1$. The minimum values of w_{pend} are between 4-6% for the three chain lengths.

The fraction of network single-chain loops vs. r plotted in Figure 9 shows that it exhibits a maximum for all three chain lengths. The maximum occurs at $r = 1.05$ for the 10-mer system and $r = 1$ for the 20- and 50-mer systems. The values for the maximum w_{loops} are $\sim 5\%$ for the 10- and 20-mer networks, and $\sim 2\%$ for the 50-mer networks and are comparable to the results of Leung and Eichinger⁶⁻⁷ and of Grest, et al¹². The fraction of single-chain loops decreases with increasing chain length because intramolecular reactions occur more favorably with shorter chains. The lowest fraction of loops occurs at the highest r values because the abundance of cross-links at these values does not favor loop formation.

The fraction of elastic chains is plotted versus r in Figure 10. There are clear maxima in the fraction of elastic chains for each chain length. For the 10-mer network the maximum appears to be at $r = 1.05$, for the 20-mer network, the maximum appears to be between $r = 1.05$ and 1.2, and for the 50-mer networks, the maximum is at $r = 1.2$. The 50-mer networks has the highest w_{elast} of almost 92%. These r values at which w_{elast} is a maximum correspond to where the w_{sol} values are at a minimum within the error bars for each of the chain lengths studied. This result is also observed experimentally⁵.

Also in Figure 10, the fraction of elastic chains is compared with results from the Macosko & Miller nonlinear polymerization theory³⁰⁻³² for the 10-mer and 50-mer systems. An average extent of reaction was determined from the four trial runs of the simulation for each value of r and each chain length. These average extents of reaction were then used as input to the Macosko & Miller theory to calculate the fraction of elastic material. Qualitatively, the theory matches the simulation results in that there is a maximum in the fraction of elastic material at $r > 1$ for all chain lengths and that the maximum appears to shift to higher r values with increasing chain length. The actual values of w_{elast} for the theory are higher than the simulation however, because the theory does not take into account loop formation and determines the pendent material indirectly. Although theoretical models have been developed which include intramolecular reactions in nonlinear copolymerization reactions³³⁻³⁵, these theories require solving sets of differential equations and calculation of additional parameters.

Figure 11 shows the soluble fraction versus r for the 50-mer systems that were allowed to cure with a cross-link-cross-link side reaction with a reaction probability, $P_x = 0.25$, and without a side reaction, $P_x = 0.0$. For the networks with side reaction, the w_{sol}

values appear to level off to a constant value (within the error bars) for $r \geq 1.4$. This indicates that side reactions do indeed shift the r_{opt} value to higher r values. The average w_{sol} value at which the plateau occurs is approximately 0.1%, which is lower than w_{sol} for the system without a side reaction which is 0.3%. This plot does not exhibit a clear minimum as is apparent in the system studied without a side reaction, because the cross-links can keep on reacting with each other as the cure progresses. Such trends are also observed experimentally. For example, for PDMS networks formed from vinyl-terminated precursor chains of molecular weight 18.5K and tetrakis(dimethylsiloxy)silane cross-links, a sharp r_{opt} at 1.69 is observed where $w_{sol} = 1.21\%$ ¹. In this case, the extent of side reaction is expected to be small and on the order of 10%³. On the other hand, for PDMS networks of hydroxyl-terminated precursor chains of molecular weight equal 17.7K with tetraethylorthosilicate (TEOS) cross-links, no sharp r_{opt} is observed⁵. Instead, w_{sol} values reach a plateau at approximately 0.7% over the range of $r = 2$ to 5. In this case, TEOS reacts with itself extensively and gets incorporated in the network causing the soluble fraction for low polydispersity PDMS precursors to remain negligible for an extremely wide range of r values.

Conclusions

End-linked networks of 10-, 20-, and 50-mer precursor polymer chains were created with a wide range of cross-link concentrations using the athermal bond fluctuation model in three dimensions. The 10- and 20-mer networks were studied on a 60x60x60 lattice and the 50-mer networks on a 95x95x95 lattice. Networks were cured with and without a side reaction between cross-links. In order to model experimental

conditions, the cure was stopped at a constant MC step per repeat unit for all ratios of cross-links to precursor chains studied for a given chain length.

A method to catalog the network connectivity was developed to determine the soluble fraction and network defects such as loops and pendent material. This algorithm can directly determine single-chain loops, pendent chains, and branched pendent structures, which is an extension of previous work³⁰⁻³². Optimum conditions minimizing the soluble fraction and pendent material and maximizing the fraction of elastic material were determined to be $r_{opt} \sim 1.05$ for the 10-mer networks, $r_{opt} \sim 1.05 - 1.2$ for the 20-mer networks, and $r_{opt} = 1.2$ for the 50-mer networks. This effect appears to be the result of the kinetic limitation which prevents systems at lower r ($r = 0.9$ and 1.0) to achieve high extents of reaction in a reasonable cure time. For the 50-mer networks with a 25% probability of a cross-link-cross-link side reaction, the $r_{opt} \geq 1.4$.

In this study, we examined the formation and structure of both stoichiometric and non-stoichiometric polymer networks. Non-stoichiometric networks had not been studied previously using a dynamic simulation method such as Monte Carlo or molecular dynamics. We confirm experimental results that optimum r values are found at non-stoichiometric ratios, increase with increasing precursor polymer chain length, and increase with side reaction. We are extending these same techniques to the study of the molecular conformations of deformed polymer networks and of 'dilute' polymer networks, which are cured in the presence of a large fraction of unreactive linear chains.

Acknowledgements

Financial support for this work has been provided by the National Science Foundation, under grant number DMR-9706066.

References

- ¹ S.K. Patel, S. Malone, C. Cohen, J.R. Gillmor, and R.H. Colby, *Macromolecules* **25**, 5241 (1992).
- ² H. Takahashi, M. Shibayama, H. Fujisawa, and S. Nomura, *Macromolecules* **28**, 8824 (1995).
- ³ C.W. Macosko and G.S. Benjamin, *Pure & Appl. Chem.* **53**, 1505 (1981).
- ⁴ C.W. Macosko and J.C. Saam, *Polymer Bulletin* **18**, 463 (1987).
- ⁵ H. Takeuchi and C. Cohen, *Macromolecules* **32**, 6792 (1999).
- ⁶ Y-K. Leung and B.E. Eichinger, *J. Chem. Phys.* **80**, 3877 (1984).
- ⁷ Y-K. Leung and B.E. Eichinger, *J. Chem. Phys.* **80**, 3885 (1984).
- ⁸ H.L. Trautenberg, J-U. Sommer, and D. Goritz, *Macromol. Symp.* **81**, 153 (1994).
- ⁹ H.L. Trautenberg, J-U. Sommer, and D. Goritz, *J. Chem. Soc. Faraday Trans.* **91**, 2649 (1995).
- ¹⁰ T. Holzl, H.L. Trautenberg, and D. Goritz, *Phys. Rev. Lett.* **79**, 2293 (1997).
- ¹¹ E.R. Duering, K. Kremer, and G.S. Grest, *J. Chem. Phys.* **101**, 8169 (1994).
- ¹² G.S. Grest, K. Kremer, and E.R. Duering, *Europhys. Letters* **19**, 195 (1992).
- ¹³ G.S. Grest and K. Kremer, *Macromolecules* **23**, 4994 (1990).
- ¹⁴ J-U. Sommer, *Macromol. Symp.* **81**, 139 (1994).
- ¹⁵ M. Schulz, and H.L. Frisch, *J. Chem. Phys.* **101**, 10008 (1994).
- ¹⁶ J-U. Sommer, T.A. Vilgis, and G. Heinrich, *J. Chem. Phys.* **100**, 9181 (1994).
- ¹⁷ J-U. Sommer, M. Schulz, and H.L. Trautenberg, *J. Chem. Phys.* **98**, 7515 (1993).
- ¹⁸ S. Dutton, D. Rolfes, and R.T.F. Stepto, *Polymer* **35**, 4521 (1994).
- ¹⁹ R.T.F. Stepto and D.J.R. Taylor, *J. Chem. Soc. Faraday Trans.* **91**, 2639 (1995).
- ²⁰ N.R. Kenkare, S.W. Smith, C.K. Hall, and S.A. Khan, *Macromolecules* **31**, 5861 (1998).
- ²¹ N.R. Kenkare, C.K. Hall, and S.A. Khan, *J. Chem. Phys.* **110**, 7556 (1999).
- ²² F.A. Escobedo and J.J. de Pablo, *J. Chem. Phys.* **104**, 4788 (1996).
- ²³ F.A. Escobedo and J.J. de Pablo, *J. Chem. Phys.* **106**, 793 (1997).

- ²⁴ C.W. Yong and P.G. Higgs, *Macromolecules* **32**, 5062 (1999).
- ²⁵ I. Carmesin and K. Kremer, *Macromolecules* **21**, 2819 (1988).
- ²⁶ H-P. Deutsch and K. Binder, *J. Chem. Phys.* **94**, 2294 (1991).
- ²⁷ W. Paul, K. Binder, D.W. Heermann, and K. Kremer, *J. Phys. II* **1**, 37 (1991).
- ²⁸ K. Binder, in *Monte Carlo and Molecular Dynamics Simulations in Polymer Science*, edited by K. Binder (Oxford University Press, New York, 1995).
- ²⁹ A. Nijenhuis and H.S. Wilf, *Combinatorial Algorithms* (Academic Press, San Diego, 1975).
- ³⁰ D.R. Miller, E.M. Valles, and C.W. Macosko, *Polym. Eng. and Sci.* **19**, 272 (1979).
- ³¹ C.W. Macosko and D.R. Miller, *Macromolecules* **9**, 199 (1976).
- ³² D.R. Miller and C.W. Macosko, *Macromolecules* **9**, 206 (1976).
- ³³ C. Sarmoria, E. Valles, and D.R. Miller, *Macromol. Chem., Macromol. Symp.* **2**, 69 (1986).
- ³⁴ M.S. Di Nezio, C. Sarmoria, and E.M. Valles, *Polymer* **39**, 4037 (1998).
- ³⁵ H. Rolfes and R.T.F. Stepto, *Makromol. Chem., Macromol. Symp.* **65**, 233 (1993).

Figure Captions

Figure 1: Terminal points of the network used to determine pendent structures: a) end-capped chain, b) dangling loop, c) dangling chain(s). The squares represent cross-links and the lines represent polymer chains. The arrow indicates a connection to the network.

Figure 2: Fraction of unreacted chain ends versus Monte Carlo steps per repeat unit (MCS/RU) for the 50-mer networks as a function of the ratio r . The thin, straight line represents a line of slope -0.5 .

Figure 3: Soluble fraction, w_{sol} , versus Monte Carlo steps per repeat unit (MCS/RU) for the 50-mer networks as a function of the ratio r .

Figure 4: Fraction of pendent material, w_{pend} , versus Monte Carlo steps per repeat unit (MCS/RU) for the 50-mer networks as a function of the ratio r .

Figure 5: Fraction of single-chain loops, w_{loops} , versus Monte Carlo steps per repeat unit (MCS/RU) for the 50-mer networks as a function of the ratio r .

Figure 6: Fraction of elastic material, w_{elast} , versus Monte Carlo step per repeat unit (MCS/RU) for the 50-mer networks as a function of the ratio r .

Figure 7: Soluble fraction, w_{sol} , versus the ratio, r for each chain length at a constant cure time. Lines are drawn through the points for visual clarity.

Figure 8: Fraction of pendent material, w_{pend} , versus the ratio, r , for each chain length at a constant cure time. Lines are drawn through the points for visual clarity.

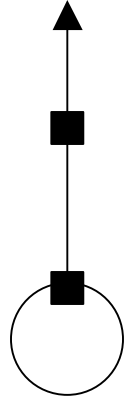
Figure 9: Fraction of single-chain loops, w_{loops} , versus the ratio, r , for each chain length at a constant cure time. Lines are drawn through the points for visual clarity.

Figure 10: The fraction of elastic material, w_{elast} , versus the ratio, r , for each chain length at a constant cure time. Interrupted lines are drawn through the simulation points for visual clarity. Continuous lines are from the Macosko and Miller theory for 10- and 50-mer systems.

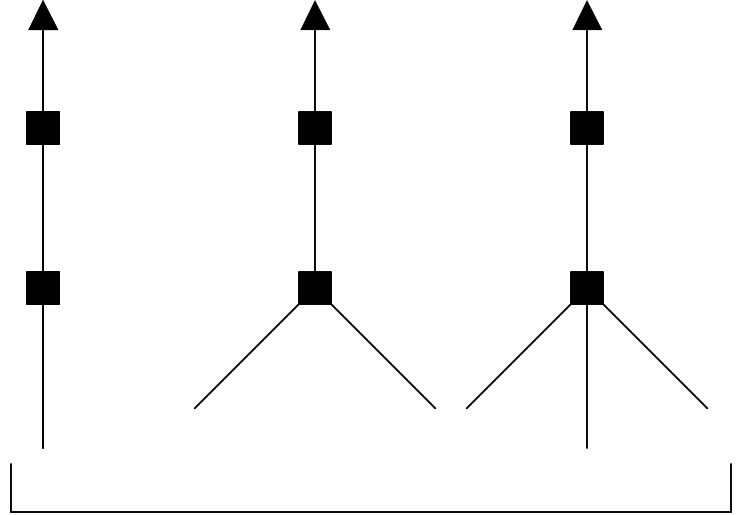
Figure 11: Soluble fraction, w_{sol} , versus the ratio, r , for the 50-mer networks with and without a side reaction. P_x is the probability of side reaction. Lines are drawn through the points for visual clarity.



a



b



c

